Control of the Evolution of Iron Peroxide Intermediate in Superoxide Reductase from *Desulfoarculus baarsii*. Involvement of Lysine 48 in Protonation

Florence Bonnot,[†,‡,§] Thibaut Molle,[†,‡,§] Stéphane Ménage,[†,‡,§] Yohann Moreau,[†,‡,§] Simon Duval,[†,‡,§] Vincent Favaudon,[∥] Chantal Houée-Levin,[⊥] and Vincent Nivière*[,†,‡,§]

[†]CEA, iRTSV, Laboratoire de Chimie et Biologie des Métaux, F-38054 Grenoble, France
[‡]Université de Grenoble, F-38000 Grenoble, France
[§]CNRS, UMR 5249, F-38054 Grenoble, France
[∥]Institut Curie, Inserm U612, Bâtiment 110-112, Centre Universitaire 91405 Orsay Cedex, France
[⊥]Laboratoire de Chimie Physique, UMR8000 CNRS/Université Paris-Sud, Bâtiment 350, Centre Universitaire 91405 Orsay Cedex, France

Ⓢ Supporting Information

ABSTRACT: Superoxide reductase is a nonheme iron metalloenzyme that detoxifies superoxide anion radicals $O_2^{\bullet-}$ in some microorganisms. Its catalytic mechanism was previously proposed to involve a single ferric iron (hydro)peroxo intermediate, which is protonated to form the reaction product H_2O_2. Here, we show by pulse radiolysis that the mutation of the well-conserved lysine 48 into isoleucine in the SOR from *Desulfoarculus baarsii* dramatically affects its reaction with $O_2^{\bullet-}$. Although the first reaction intermediate and its decay are not affected by the mutation, H_2O_2 is no longer the reaction product. In addition, in contrast to the wild-type SOR, the lysine mutant catalyzes a two-electron oxidation of an olefin into epoxide in the presence of H_2O_2, suggesting the formation of iron-oxo intermediate species in this mutant. In agreement with the recent X-ray structures of the peroxide intermediates trapped in a SOR crystal, these data support the involvement of lysine 48 in the specific protonation of the proximal oxygen of the peroxide intermediate to generate H_2O_2, thus avoiding formation of iron-oxo species, as is observed in cytochrome P450. In addition, we proposed that the first reaction intermediate observed by pulse radiolysis is a ferrous-iron superoxo species, in agreement with TD-DFT calculations of the absorption spectrum of this intermediate. A new reaction scheme for the catalytical mechanism of SOR with $O_2^{\bullet-}$ is presented in which ferrous iron-superoxo and ferric hydroperoxide species are reaction intermediates, and the lysine 48 plays a key role in the control of the evolution of iron peroxide intermediate to form H_2O_2.
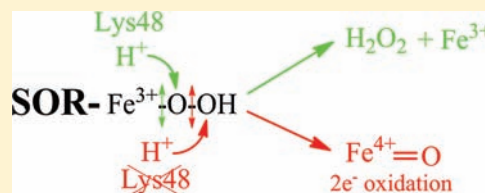
■ INTRODUCTION

Detoxification of the superoxide anion radical $O_2^{\bullet-}$ is one of the main processes that allows the cells to withstand oxidative stress.[1,2] Superoxide dismutase (SOD) has long been considered as the sole enzymatic system able to eliminate $O_2^{\bullet-}$, by catalyzing its dismutation into H_2O_2 and O_2.[3] Recently, however, evidence for the existence of an alternative enzymatic system to detoxify $O_2^{\bullet-}$ was discovered in some specific bacteria.[4,5] This enzyme, called superoxide reductase (SOR), catalyzes the reduction of $O_2^{\bullet-}$ into H_2O_2 without production of O_2.

$$O_2^{\bullet-} + 1e^- + 2H^+ \rightarrow H_2O_2 (SOR)$$
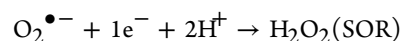
Unlike SOD, SOR requires a source of electrons to reduce $O_2^{\bullet-}$, which can be provided by cellular reductases and/or soluble electron transfer proteins.[6−8] Although SODs and SORs are structurally unrelated, they are both able to react with $O_2^{\bullet-}$ at a nearly diffusion-controlled rate, and SOR has

appeared as efficient as SOD to protect cells from $O_2^{\bullet-}$-induced stress.[6]

SORs, also known as desulfoferrodoxin or neelaredoxin, are small iron metalloproteins, which all contain the same active site.[9−12] It consists of a mononuclear ferrous iron site, in an atypical $[FeN_4S_1]$ coordination, where the nitrogen ligands are provided by four histidine residues and the sulfur ligand, in an axial position, by a cysteine residue.[13,14] A similar $[FeS_1N_4]$ coordination is also present in the active site of cytochrome P450, with however the presence of a porphyrin ring instead of histidine ligands.[15] Different classes of SOR have been described, depending on the presence of additional structural domains.[9−12] The enzyme from *Desulfoarculus baarsii* presents an additional N-terminal domain, which contains a second mononuclear iron center $[Fe^{3+}(Cys)S_4]$, similar to that found in desulforedoxin.[5,12,14] It was recently proposed that this iron

center serves as an electron relay between some peculiar electron donor proteins and the active site.[16,17]

The mechanism of the reduction of $O_2^{\bullet-}$ by SOR has been extensively studied by rapid kinetics studies, mainly by means of pulse radiolysis.[18−21] A first reaction intermediate T1 would be a Fe^{3+}−O−O(H) species resulting from an inner-sphere reduction mechanism of $O_2^{\bullet-}$ by the ferrous iron. This is in agreement with the capability of the SOR active site to accommodate Fe^{3+}−O−O(H) species when reacted with H_2O_2,[22−25] and with a synthetic SOR model to form such species when reacted with $O_2^{\bullet-}$.[26] The intermediate T1 decays through a process ending in the formation and the release of the H_2O_2 product from the active site. Protonation processes are central in SOR catalysis because two protons, in addition to one electron, are required to form H_2O_2 from $O_2^{\bullet-}$. However, rapid kinetic studies have identified only one catalytic competent protonation step, which is involved in the decay of T1.[18−21] The rate constant of the decay of T1 in acidic medium is proportional to the concentration of protons in solution, suggesting a direct protonation of T1 by H_3O^+ from the bulk solvent.[18−21] At the end of the reaction, SOR lies in a Fe^{3+} hexacoordinated resting state, in which the carboxylate side chain of the E47 residue (according to the numbering of the *D. baarsii* enzyme) occupies the sixth coordination position.[18−21]

Recently, X-ray structures of iron peroxide species trapped in the active site of the SOR from *D. baarsii* have suggested a specific role for the lateral chain of the K48 residue in the control of protonation process during SOR catalysis.[25] Actually, K48, a well-conserved residue among SORs, is located at the surface of the protein in a conformation depending on the redox state of the active site.[13] In the ferrous state, where its neighbor residue E47 is not bound to iron, K48 is located at about 6 Å from the iron atom.[13] Such close proximity of K48 was proposed to induce an electrostatic attraction of the negative charged $O_2^{\bullet-}$ to the iron site, contributing to the very fast formation of the T1 intermediate.[18,19] In the ferric state, where E47 becomes a ligand of the iron, K48 moves away from the iron site, at 12 Å distance.[13] In the iron peroxide state, K48 can adopt different conformations around the peroxide moiety.[25] In one conformation, K48, through hydrogen bond, positions a water molecule at a distance compatible with a hydrogen bond to the proximal oxygen of the hydroperoxo species.[25] This suggests a mechanism involving K48 to specifically protonate the proximal oxygen of the iron-hydroperoxo intermediate to generate H_2O_2. Interestingly, in cytochrome P450, which also forms an iron-hydroperoxo intermediate during its catalytic cycle, a hydrogen-bond network drives the protonation of the distal oxygen of the iron-hydroperoxo species. This facilitates the heterolytic cleavage of the O−O bond of the peroxide,[15] which leads to the formation of a high-valent iron-oxo intermediate. The iron-oxo species is responsible for the oxidation of substrates by cytochrome P450.[15] In SOR, K48, by inducing the protonation of the proximal oxygen, might favor the cleavage of the Fe−O bond of the peroxide intermediate to form H_2O_2, thus avoiding formation of iron-oxo species in its active site.[25] However, experimental evidence in support of such a function of K48 in SOR catalysis is lacking. Previous studies on K48 SOR mutants from *D. baarsii* and *Desulfovibrio vulgaris* Hildenborough did not reveal any significant alteration of the protonation step observable by pulse radiolysis.[18,19] Nevertheless, recently, we showed that for the wild-type (wt) SOR from *D. baarsii* at pH

7.6, the reaction intermediate T1 is highly susceptible to be photodegradated by the intense light beam used in pulse radiolysis experiments below 345 nm.[21] This photochemical process affects the absorption spectrum of a late reaction intermediate, together with the kinetics of its evolution to the final reaction product.[21] The absence of effects of the K48I mutation on the reactivity of SOR with $O_2^{\bullet-}$ described in these studies then is questionable and deserves more investigations. These remarks also apply for the E47A SOR mutant from *D. baarsii*, which was previously reported to have no effects on catalysis.[19] The effects of this mutation also need reinvestigation in the absence of the photochemical process, in particular to allow a better analysis of the specific role of the K48 residue in catalysis.

Here, the reactions of the wt, E47A, and K48I SORs from *D. baarsii* with $O_2^{\bullet-}$ were reinvestigated by pulse radiolysis at different pH's between 5.5 and 10.2 using a 345 nm cutoff filter on the light beam to avoid any photochemical side reactions.[21] The study reveals that the formation of the first reaction intermediate T1 was not affected by the K48I mutation. However, this mutation drastically impacts the reactivity of SOR toward $O_2^{\bullet-}$ through the control of a specific protonation step of the proximal oxygen of the iron hydroperoxide intermediate to produce H_2O_2. These data suggest that in the K48I SOR mutant, a high valent iron-oxo species can be formed in the active site.

■ EXPERIMENTAL PROCEDURES

Materials. Sodium formate and buffers were of the highest quality available (Prolabo Normatom or Merck Suprapure). Oxygen was from ALPHA GAZ. Its purity was higher than 99.99%. Water was purified using an Elga Maxima system (resistivity 18.2 MΩ). K_2IrCl_6 was from Strem Chemical Inc. Benzophenone was from Aldrich (99%).

Protein Purifications. Overexpressions and purifications of the wt, E47A, and K48I SOR mutants from *D. baarsii* were carried out as reported previously.[19,21]

Pulse Radiolysis. Pulse radiolysis measurements were performed as described elsewhere.[21] Briefly, free radicals were generated by irradiation of O_2-saturated ($[O_2] \approx 1$ mM) aqueous protein solutions (100 μM), in 2 mM buffer, 10 mM sodium formate with 0.2−2 μs pulses of 4.5 MeV electrons at the linear accelerator at the Curie Institute, Orsay, France. $O_2^{\bullet-}$ was generated from reduction of O_2 by the carboxyl radical formed during the scavenging by formate of the $HO^{\bullet}$ radical.[27] The doses per pulse were calibrated from the absorption of the thiocyanate radical $(SCN)_2^{\bullet-}$ obtained by radiolysis of 10 mM KSCN in N_2O-saturated solution ($G = 0.55$ μmol J^{-1}, $\varepsilon_{472\,nm} = 7580$ M^{-1} cm^{-1}).[27] The radiation dose varied linearly with the pulse length; for instance, a 0.2 μs long pulse yielded a dose of ca. 5 Gy ($[O_2^{\bullet-}] \approx 2.8$ μM). Reactions were followed spectrophotometrically, using a 150 W continuous Hamamatsu SuperQuiet xenon−mercury arc (310−750 nm) or a tungsten lamp (450−750 nm), at 20 °C in a 2 cm path-length fused silica cuvette. A cutoff filter cutting all wavelengths below either 345 nm or 425 nm was positioned between the lamp and the cuvette.[21] Identical results were obtained with the 345 and the 425 nm filters. The kinetics of the reaction was followed spectrophotometrically between 450 and 700 nm on the microsecond to second time scale. The proteins were present in large excess with regard to $O_2^{\bullet-}$, providing pseudo first-order conditions. Kinetic traces were analyzed using a Levenberg−Marquardt algorithm from the Kaleidagraph software package (Synergy Software).

pH Studies. The following different buffers were used to cover the pH range 5.5−10.2: pH 5.5, acetate buffer; pH 5.6, 6.0, 6.5, MES buffer; pH 7.0, bis-Tris propane or HEPES buffer; pH 7.6, 8.1, 8.5, 8.8, Tris-HCl buffer; pH 9.1, 9.5, 10.2, 10.5, glycine-NaOH buffer.

Electrospray Ionization Mass Spectroscopy. Electrospray ionization mass spectra were obtained on a Perkin-Elmer Sciex API III+ triple quadrupole mass spectrometer equipped with a nebulizer-

assisted electrospray source operating at atmospheric pressure. Samples were made in 10 mM ammonium acetate.

Hydrogen Peroxide. Hydrogen peroxide was determined immediately after irradiation using the leuco crystal violet horseradish peroxidase method.[28]

Oxidation of 2-Cyclohexen-1-ol. In a standard reaction, 0.05–5 mM of H_2O_2 was mixed with 100 μM of SOR, 3 mM 2-cyclohexen-1-ol, and 0.4 M ethanol, in 10 mM Tris/HCl buffer pH 8.5, 100 μL final volume. The reaction was performed under a 100% nitrogen atmosphere (inert gloves box system Jacomex), at room temperature. After 2–10 min incubation, 10 μL of 0.1 mM benzophenone 99% diluted with dichloromethane was added as a reference. The reaction mixture was then extracted with dichloromethane. The organic phase was concentrated under vacuum until a volume of 5–10 μL and injected into the gas chromatography apparatus (GC). The products were identified by comparison of their GC retention times with those of authentic synthetic compounds. For 7-oxabicyclo[4-1-0] heptan 2-ol (also named 1,2-epoxycyclohexan-3-ol, the product of 2-cyclohexen-1-ol epoxidation), two peaks were detected, corresponding to the two enantiomers *syn* and *anti*. The peak of each enantiomer was identified thanks to the synthetic epoxides, which were obtained using peroxy acid, described to form the two enantiomers *syn* and *anti* in a ratio of 91:9 *syn:anti*.[29] The gas chromatography apparatus was a PerkinElmer Autosystem (Optima-17 column, 30 m), connected to a PE Nelson 1022 integrator with flame-ionization detector. The temperature program started at 100 °C for 4 min and then increased 25 °C per min.

Computations. Calculations were performed using the Gaussian 03 package.[30] Geometries were optimized in vacuum with the B3LYP hybrid density functional[31,32] and using a double-ζ quality basis set using 6-31G* for C, H, N, O, and S atoms, while a lanl2dz with ECP,[33] augmented with an f polarization function of exponent 3.25, was used for iron. The model systems were taken from the crystallographic structure of the wt SOR (Protein Data Bank code: 2JI1).[25] To build the systems, only the five amino acids binding iron were considered, H49, H69, H75, H119, and C116. For each amino acid, only the side chain plus α-carbons were kept and saturated by hydrogens to replace neighboring N and C atoms of the backbone. During the geometry optimization, Cα were kept fixed at their crystallographic positions, while hydrogens bound to them were free to move only along the Cα–N or Cα–C direction found in the crystallographic structure. By doing so, the arrangement of the active site and the local constraints imposed by the protein structure during geometry optimizations were conserved. Two systems were considered here: the pentacoordinated with iron at a formal oxidation degree of +II (no $O_2^{\bullet-}$ bound), and the hexacoordinated state, with one $O_2^{\bullet-}$ bound to the ferrous iron. UV/visible spectra were obtained by means of TD-DFT methodology.[34,35] Single point calculations were done on the preoptimized structures at the B3LYP/6-311+G** level of theory, as implemented in the Gaussian package. The effects of the protein environment on the active site were accounted for by means of the PCM implicit model of solvent[36] with a dielectric constant of 4.0 and an increased probe radius of 2.7 Å, so as to avoid any overpolarization problems due to the presence of diffuse basis functions. For each structure, the 20 transitions of lowest energy were computed (keyword TS=NStates=20).

■ RESULTS AND DISCUSSION

Formation of the T1 Intermediate in the Absence of Photochemical Processes. The reaction of the wt, E47A, and K48I SOR mutants from *D. baarsii* with $O_2^{\bullet-}$ was investigated by pulse radiolysis at different pH's between 5.5 and 10.2. A 345 nm cutoff filter was placed on the analysis light beam to prevent any photochemical reaction.[21] For the three reduced proteins, the reaction conduced to the formation of a first reaction intermediate, named T1, with a rate constant k_1 (Scheme 1), independent of the pH between 5.5 and 10.2 (data not shown). These data are similar to those reported previously

Scheme 1. Reaction Mechanism of the SOR from *D. baarsii* with $O_2^{\bullet-}$ Deduced from Pulse Radiolysis Studies[a]
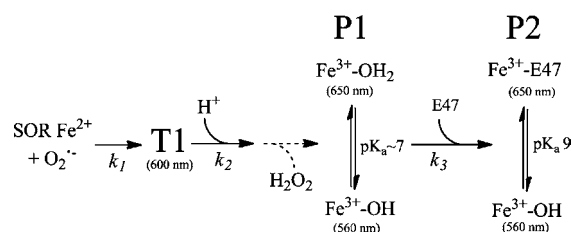
[a]T1 is the only competent reaction intermediate observed by pulse radiolysis. P1 and P2 are reaction products formed after the release of H_2O_2 from the active site.

in the absence of the 345 nm filter.[19] Formation of T1 corresponded to a bimolecular reaction of SOR with $O_2^{\bullet-}$ with a rate constant k_1 of $(1.0 \pm 0.2) \times 10^9$ M^{-1} s^{-1} for both the wt and the E47A SORs and of $(4.2 \pm 0.3) \times 10^7$ M^{-1} s^{-1} for the K48I SOR (data not shown). This latter value is 25 times lower than that reported for the wt protein, in agreement with an electrostatic guidance of $O_2^{\bullet-}$ by the positively charged K48 side chain, as was previously reported.[18,19]

The absorption spectra of T1 at the reaction time corresponding to its maximal formation (100 μs for both wt and E47A SORs and 1.2 ms for the K48I SOR) exhibited a similar broad absorption band centered at 600 nm, with a molar absorption coefficient value of ca. 2.5 mM^{-1} cm^{-1} (Figure 1).
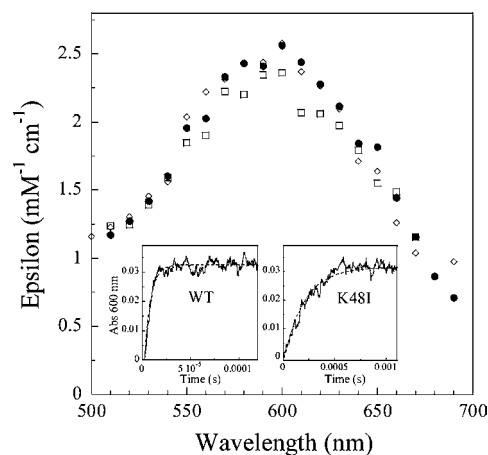

Figure 1. Transient absorption spectrum (xenon lamp with a 345 nm cutoff filter, 2 cm path-length cuvette) of the first reaction intermediate T1 for the wt (●), E47A (◇), and K48I (□) SORs, formed 100 μs (wt and E47A) or 1.2 ms (K48I) after the pulse. Proteins were 100 μM in 10 mM formate, 2 mM Tris-HCl pH 7.6. $O_2^{\bullet-}$ concentration formed in the pulse (11 Gy) was 6.5 μM. The inset shows the time-dependent optical changes at 600 nm during the reaction of the wt and K48I proteins with $O_2^{\bullet-}$. The dashed lines were calculated for best fit to an exponential model.

In all cases, the T1 spectrum remained unaffected by the pH, between 5.5 and 9.5 (data not shown), as reported previously in the absence of the 345 nm filter.[19]

pH Dependence of the Decay of T1. The decay of T1 (rate constant k_2, Scheme 1) was independent of the enzyme concentration (data not shown). As shown in Figure 2, between pH 5.5 and 8, for the three proteins, log k_2 exhibited a linear dependence versus pH, with a slope of 0.50 ± 0.08, 0.60 ± 0.02, and 0.70 ± 0.05 for the wt, E47A, and K48I SORs,
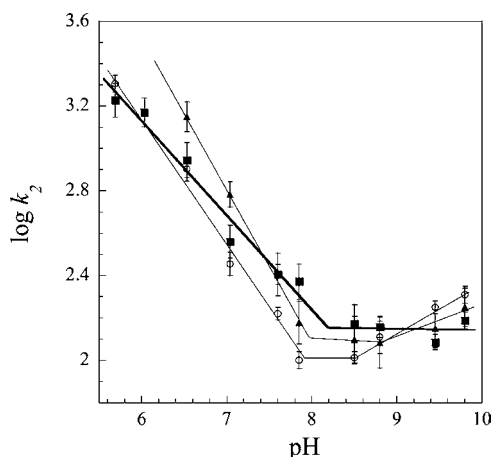
Figure 2. pH-dependence of the rate constant k_2 for the reaction of SORs from *D. baarsii* (100 μM) with $O_2^{\bullet-}$ (3 μM), generated by pulse radiolysis in the presence of 10 mM formate and 2 mM buffer. Xenon lamp with a 345 nm cutoff filter. (■, bold line), wt SOR; (○, thin line), E47A SOR mutant; (▲, dashed line), K48I SOR mutant. In the range 5.5 < pH < 8.0, log k_2 values were fitted to a linear equation, log $k_2 = \log k_0 - \alpha$pH, $\alpha = 0.50 \pm 0.08$ and $k_0 = (1.5 \pm 1.5) \times 10^6$ s^{-1} (wt SOR), $\alpha = 0.60 \pm 0.02$ and $k_0 = (4.7 \pm 1.0) \times 10^6$ s^{-1} (E47A SOR mutant), $\alpha = 0.70 \pm 0.05$ and $k_0 = (7.5 \pm 2.0) \times 10^7$ s^{-1} (K48I SOR mutant). k_0 is the limit of the protonation rate constant when pH values approach zero.

respectively.[37] These values of slope are consistent with a rate-limiting protonation process in the decays of T1, with a proton coming from the H_3O^+ bulk solvent. Above pH 8 and up to pH 10, k_2 became independent of the H^+ concentration for the wt SOR. Such a pH-independent process was also reported for the enzymes from *D. vulgaris* and *Archeoglobus fulgidus* and was proposed to involve a water molecule in the protonation process in more basic medium.[18,20] Conversely, for the E47A and K48I proteins, k_2 increased slightly with the pH (Figure 2). This might reflect some favorable effect of the deprotonation of surrounding residues on that step, or the involvement of HO^-. Nevertheless, these data confirm that the E47A and K48I mutations do not impact the kinetics of the decay of T1, which clearly remained in acidic and neutral media associated with a rate-limiting protonation process involving H_3O^+.

Absorption Spectra of the Transient P1 and the Final Species P2. For the wt protein at pH 7.6, the decay of T1 (rate constant k_2) was previously shown to result in the formation of a second transient, renamed here P1, which then evolved to the final SOR−Fe^{3+}−E47 species, P2 (rate constant k_3, Scheme 1). The spectra of P1 and of P2 were determined at different pH's between 6 and 9.5 (Figure 3). Because P1 evolved toward the formation of P2 before its maximal formation, the spectrum of P1 was calculated by an extrapolation of the kinetic traces at wavelengths between 500 and 700 nm, using k_2 and k_3 values given in Figures 2 and 4 (see above). The spectrum of P2 was reconstructed from the absorbance value at different wavelengths at the end of the reaction.

As shown in Figure 3, the absorption spectra of P1 and P2 varied with pH. For both species, their absorption maxima shifted from 650 nm (pH < 8.5) to 560 nm (pH 9.5) and were superimposable to those reported for the alkaline transition of the SOR ferric active site.[19] The alkaline transition is associated with an acid−base equilibrium between the Fe^{3+}−E47 (wt SOR) or the Fe^{3+}−OH_2 (E47A mutant) species present in
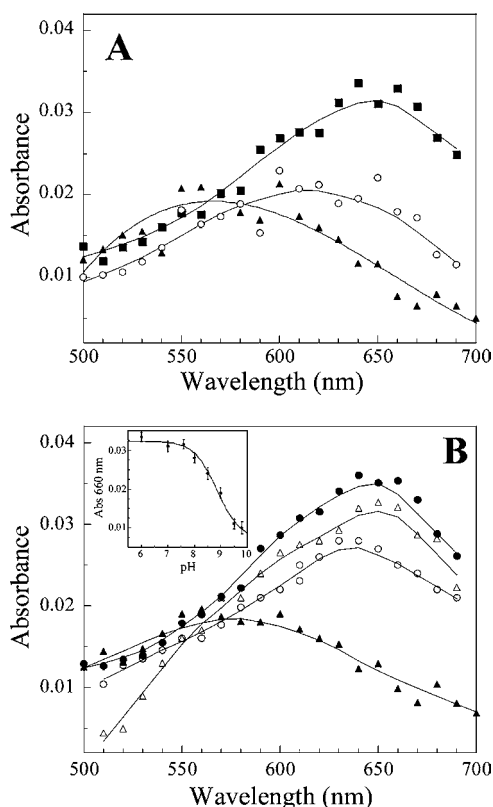

Figure 3. Absorption spectra (tungsten lamp with a 345 nm cutoff filter, 2 cm path-length cuvette) at various pH values of the P1 transient and of the final species P2 formed after the reaction of the SOR wt from *D. baarsii* with $O_2^{\bullet-}$ (8 μM), generated by pulse radiolysis in the presence of 10 mM formate and 2 mM buffer. (A) Spectra of P1 at pH 6.0 and 5 ms after the pulse (■), pH 8.5 and 50 ms after the pulse (○), and pH 9.5 and 60 ms after the pulse (▲). The spectra were calculated from an extrapolation of the decay of T1, using the double exponential fits of the kinetic traces at different wavelengths: $A = A_1 \exp(-k_2{}^*t) + A_2 \exp(-k_3{}^*t) + A_3$, where A is the absorbance at time t; A_1 and A_2 are pre-exponential terms that describe the amplitude of each phase associated with k_2 and k_3, respectively; and A_3 is the absorbance at the end of the reaction. A_2+A_3 corresponds to the absorbance of P1 at a specific wavelength. (B) Experimental spectra of P2 at pH 6.0 and 40 ms after the pulse (●), pH 7.6 and 70 ms after the pulse (△), pH 8.5 and 200 ms after the pulse (○), and pH 9.5 and 800 ms after the pulse (▲). The inset shows the pH dependence of the absorbance at 660 nm. The titration curve fitted the equation expected from a single protonation process, $A_{660 \text{ nm}} = (A_{660\text{max}} + A_{660\text{min}} \times 10^{(\text{pH}-pK_a)})/(1 + 10^{(\text{pH}-pK_a)})$. A p$K_a$ value of 8.9 ± 0.2 was determined.

acidic medium (band at 650 nm) and the Fe^{3+}−OH species present in more basic medium (band at 560 nm).[19,38] For P1, taking into account the uncertainty associated with the calculation of its spectrum, in particular at neutral pH (in this pH domain, k_2 and k_3 values were close to each other), a pK_a value for the 650−560 nm transition could not be determined accurately. For P2, the 650−560 nm transition appeared to occur with a pK_a value of 8.9 ± 0.2 (inset of Figure 3B), similar to that reported for the SOR ferric active site.[19] These data are fully consistent with the formation of the Fe^{3+}−E47/Fe^{3+}−OH species at the end of the reaction. Comparison of the spectra of P1 and of the Fe^{3+}−E47/Fe^{3+}−OH final species at different pH's (Figure 3A and B) suggests however that the pK_a of the P1 transition is lower than that of P2.
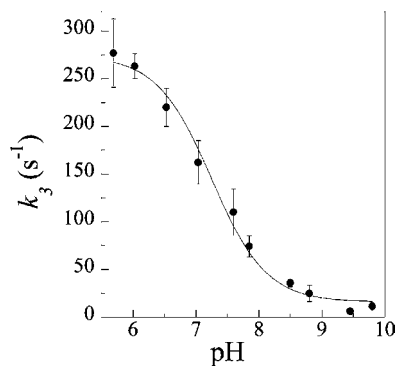
Figure 4. pH-dependence of the rate constant k_3 for the reaction of the wt SOR from *D. baarsii* (100 μM) with $O_2^{\bullet-}$ (8–12 μM), generated by pulse radiolysis in the presence of 10 mM formate and 2 mM buffer. Tungsten lamp with a 345 nm cutoff filter. The titration curve fitted the equation expected from a single protonation process, $k_3 = (k_{3max} + k_{3min} \times 10^{(pH-pK_a)})/(1 + 10^{(pH-pK_a)})$. A p$K_a$ value of 7.2 ± 0.1 was determined.

The decay of P1 into P2 (rate constant k_3, Scheme 1) was found to be independent of the enzyme concentration (data not shown). As shown in Figure 4, the rate constant k_3 varied with pH, with a pK_a value of 7.2 ± 0.1.

P1 as the Final Species for the E47A SOR Mutant. For the E47A mutant, at all of the pH's investigated between 5.5 and 10.2, the decay of T1 (k_2) led directly to the formation of a final species, without evidence of a third reaction step (no k_3 observed). The absorption spectrum of the final species was reconstructed at pH 5.5 and 8.5 and was found to be superimposable to that of the final oxidized E47A mutant at the same pH, with a maximum of absorption shifted from 650 nm at pH 5.5 to 560 nm at pH 8.5 (Figure 5A). These spectra appeared similar to those of P1 in the wt protein, taking into account the uncertainty associated with the calculation the spectra of P1 (Figure 3A). As shown in Figure 5B, the dependence of the final absorbance at 640 nm on the pH allowed one to calculate a pK_a value of 6.7 ± 0.2 for the transition between the 650 and 560 nm absorbing species. This value is identical to the pK_a reported for the similar spectral transition of the E47A SOR ferric site, corresponding to a Fe^{3+}–OH_2/ Fe^{3+}–OH acid–base equilibrium.[19,38]

Thus, for this mutant, P1 is identified to the couple Fe^{3+}–OH_2/ Fe^{3+}–OH (Scheme 1). Because the third reaction (rate constant k_3) was specifically abolished by the E47A mutation, the formation of P2 can be associated with the binding of the E47 carboxylate group on P1, displacing the OH/OH_2 ferric iron ligand. The dependence of the rate constant k_3 on the pH (Figure 4) most likely reflects a more favorable ligand exchange of the E47 with the –OH_2 species than with the –OH species. Thus, the pK_a associated with the rate constant k_3 (P1→P2) can be associated with the Fe^{3+}–OH_2/Fe^{3+}–OH acid–base equilibrium on P1 (Scheme 1). Accordingly, its value (7.2 ± 0.1, Figure 4) is close to the pK_a value determined for the alkaline transition of the ferric E47A SOR mutant (6.7 ± 0.2).[19] It should be noted that because k_3 was still observed at pH > 9.5 (Figure 4), P1 and P2 species could not be in equilibrium with a same Fe^{3+}–OH species (Scheme 1). Thus, although the Fe^{3+}–OH species in P1 and P2 exhibit similar absorption spectra, they may not be equivalent, with a slightly different protein environment.
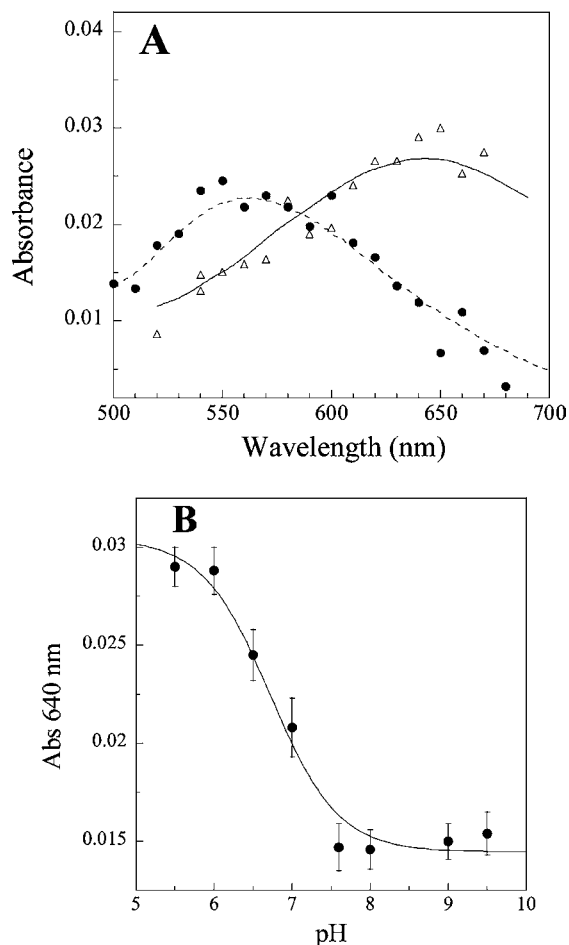

Figure 5. (A) Absorption spectra of the final species formed at different pH's after the reaction of the E47A SOR mutant with $O_2^{\bullet-}$ (8 μM), generated by pulse radiolysis in the presence of 10 mM formate and 2 mM buffer. (△) pH 5.5, 4 ms after the pulse. (●) pH 8.5, 80 ms after the pulse. Tungsten lamp with a 345 nm cutoff filter, 2 cm path-length cuvette. The absorption spectrum in the 2 cm path-length cuvette of the iridium chloride oxidized E47A SOR mutant (8 μM) is shown at pH 5.5 (—) and at pH 8.5 (- - -). (B) pH-dependence of the final absorbance at 640 nm measured after the reaction of the E47A SOR mutant from *D. baarsii* (100 μM) with $O_2^{\bullet-}$ (8 μM), under the same conditions. The titration curve fits the equation expected from a single protonation process, $A_{640\,nm} = (A_{640max} + A_{640min} \times 10^{(pH-pK_a)})/(1 + 10^{(pH-pK_a)})$. A p$K_a$ value of 6.7 ± 0.2 was determined.

Scheme 1 summarizes the reaction mechanism of SOR from *D. baarsii*, as deduced from pulse radiolysis studies on the wt and E47A proteins in the absence of photochemical process. This reaction scheme appears very similar to that reported for the SORs from *A. fulgidus*,[20] suggesting, as discussed in previous work,[21] an overall common reaction mechanism for the different SORs studied so far. It is important to underline that according to Scheme 1, T1 appeared as the only competent reaction intermediate observed by pulse radiolysis. In fact, P1, associated with a Fe^{3+}–OH_2 or Fe^{3+}–OH species, is a reaction product, resulting from the release of H_2O_2 from the active site. Actually, only one catalytic protonation step (rate constant k_2) was observed by pulse radiolysis. Thus, the other protonation process required to generate H_2O_2 from $O_2^{\bullet-}$ was not observed and should correspond to a nonrate-limiting step. That T1 could be already a protonated species, such as an iron hydroperoxo species, and that H_2O_2 formation might directly

result from the protonation of T1 were previously proposed.[20,39] However, formation of T1, which occurred at a nearly diffusion-controlled rate ($\sim 10^9$ M^{-1} s^{-1}), was found to be totally independent of pH from pH 5 to pH 10, thus over a variation of 100,000 times in the concentration of H$^+$ in the solution.[18-21] Consequently, formulation of T1 as a protonated species is questionable.

Formation of the Final Species for the K48I SOR Mutant. The spectrum resulting from the decay of T1 in the K48I mutant was reconstructed at different pH's (Figure 6). At
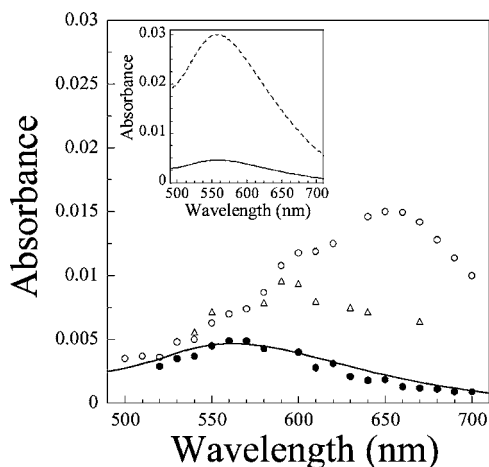

Figure 6. Absorption spectra at different pH's of the final species for the reaction of the K48I SOR mutant from *D. baarsii* (100 μM) with O$_2^{\bullet-}$ (8 μM), generated by pulse radiolysis in the presence of 10 mM formate and 2 mM buffer. Tungsten lamp with a 345 nm cutoff filter, 2 cm path-length cuvette. The spectra were reconstructed at the following pH's and times after the pulse: pH 5.6 and 20 ms (O), pH 7.6 and 500 ms ($\triangle$), and pH 8.5 and 500 ms ($\bullet$). The solid line shows the spectrum of the solution at pH 8.5 recorded on a UV–visible spectrophotometer 1 min after the pulse. The inset shows the same spectrum of the solution at pH 8.5 recorded on a UV–visible spectrophotometer 1 min after the pulse, without (–) and with treatment with a slight molar excess of K$_2$IrCl$_6$ (- - -).

pH 5.6, a spectrum similar to that of P1 was observed, with however only 40% of the intensity of that of the wt at the same pH. This species in the K48I SOR mutant evolved to an end product, which had spectral features similar to those of P2, with an intensity about 40% less than that of the wt at the same pH (data not shown). Surprisingly, when increasing the pH, in the K48I SOR mutant, the intensity of the absorbances of P1 and P2 became smaller and was almost annihilated at pH 8.5 and above (Figure 6).

Pulse radiolysis experiments were then carried out at pH 8.5, where the K48I mutant (8 μM) was reacted with a stoichiometric amount of O$_2^{\bullet-}$ (8 μM, 12.5 Gy). These conditions allowed recording directly the absorption spectrum of the solution ca. 1 min after the pulse with a classical spectrophotometer. The presence or absence of a catalytic amount of catalase added to the solution before the pulse had no effect on the final absorption spectrum (data not shown).

The solution thus obtained showed a spectrum identical to that reported in Figure 6 for the species formed at pH 8.5 and at 500 ms reaction time (($\bullet$), Figure 6). This showed that this spectrum corresponds to that of a stable final species. When the pulsed K48I SOR mutant solution at pH 8.5 was reoxidized ca. 1 min after the pulse with a slight stoichiometric excess of

K$_2$IrCl$_6$, the spectrum showed a strong increase of the band in the 560 nm region. This band was superimposable to that of a solution of K48I mutant active site (8 μM) oxidized by K$_2$IrCl$_6$ at the corresponding pH (inset of Figure 6). Electrospray mass spectra analysis of the K48I SOR mutant after the pulse radiolysis experiment gave a value of 14 010 $\pm$ 1 Da for the mass of its polypeptide chain. This value is expected for the K48I SOR mutant, showing that its polypeptide chain was not altered at the end of the reaction.

Altogether, these data indicate that the weakness or almost absence of the absorbance band at the end of the reaction of the K48I SOR mutant with O$_2^{\bullet-}$ in basic medium did not reflect a degradation of SOR, but the formation of a ferrous iron active site species. In fact, the ferrous iron site has no absorption band in the visible region.[5] Consequently, from the spectra of Figure 6 at pH 5.6, one can calculate that at the end of the reaction of the K48I mutant with O$_2^{\bullet-}$, 40% of the enzyme was oxidized (3.2 μM) and 60% reduced (4.8 μM). At pH 8.5, at the end of the reaction, 85% of the mutant was reduced (6.8 μM) and 15% oxidized (1.2 μM). The higher the pH at which the reaction of the K48I SOR mutant with O$_2^{\bullet-}$ was carried out, the more the SOR iron site ended up on a reduced state, Fe^{2+}.

Quantification of H$_2$O$_2$ production immediately after the pulse was carried out at pH 8.5 using the leuco crystal violet-horseradish peroxidase method.[28] As shown in Table 1, at pH

Table 1. Amount of H$_2$O$_2$ Produced Immediately after the Reaction of the K48I SOR Mutant (20 μM) with Various Concentrations of O$_2^{\bullet-}$, at pH 8.5

[O$_2^{\bullet-}$] reacted with SOR^a (μM)	[H$_2$O$_2$] produced^b (μM)	[H$_2$O$_2$] produced/[O$_2^{\bullet-}$] reacted with SOR (%)
3.4	0.5	15
4.4	0.4	9
6.3	1.2	19
6.8	1.2	17

^{a}O$_2^{\bullet-}$ was generated by pulse radiolysis (10 mM formate, 2 mM glycine NaOH buffer pH 8.5, 1 mM O$_2$). H$_2$O$_2$ was determined from the oxidation of LCV in the presence of horse radish peroxidise.[28] ^{b}Values were corrected from the production of H$_2$O$_2$ formed from the onset of water radiolysis ($G \approx 0.07$ μmol J^{-1}).

8.5, the formation of H$_2$O$_2$ resulting from the reaction of O$_2^{\bullet-}$ with the K48I SOR mutant represented only about 15% of the expected value for a stoichiometric reaction of SOR with O$_2^{\bullet-}$.

It should be noted that T1 was formed in the same amount in the K48I SOR mutant as compared to the wt (Figure 1). Consequently, the near-absence of the formation of H$_2$O$_2$ at basic pH's cannot be associated with the decrease of the rate constant of the reaction of the mutant with O$_2^{\bullet-}$.

Altogether, these data show that the K48I mutation has a profound effect on the reaction of SOR with O$_2^{\bullet-}$. Although the K48I mutant does not modify the spectrum of the T1 intermediate and its pH-dependent decay (Figures 1 and 2), in basic medium it does not lead to the formation of the ferric species. Instead, it leads to the formation of a ferrous SOR species, without production of H$_2$O$_2$.

Epoxidation of 2-Cyclohexen-1-ol Catalyzed by SOR: Evidence for the Formation of Iron-oxo Species in SOR. For the K48I SOR mutant, the formation of a final Fe^{2+} species without production of H$_2$O$_2$, as observed at pH 8.5 (Figure 6 and Table 1), might be the consequence of oxidation of organic

solutes present in the solution, formate, or buffer, carried out by a transient species formed at its active site. To investigate if the K48I SOR mutant could perform such oxidation reactions, we tested its ability to oxidize olefin, 2-cyclohexen-1-ol as a test substrate, in the presence of H_2O_2 at pH 8.5. Oxidation of olefins has been well described to characterize reactions catalyzed by iron complexes, in particular for those forming iron-oxo intermediates.[40−42] The reaction was conducted at room temperature under anaerobic conditions, in the presence of 5 to 50 mol equiv of H_2O_2 and 30 mol equiv of racemic 2-cyclohexen-1-ol, with respect to SOR (Table 2). In the absence

Table 2. Yields (%/SOR) of Epoxide Formation from the Oxidation of 2-Cyclohexen-1-ol by H_2O_2, in the Presence of wt, E47A or K48I SOR Mutant Proteins from *D. baarsii*[a]

SOR	H_2O_2 (equiv/SOR)	epoxide (yield/SOR)	% of destruction of SOR active site[b]
no SOR	50	0	nd
wt	5	0	nd
	10	0	∼60
	30	0	100
	50	0	100
E47A mutant	10	0	nd
	30	0	nd
K48I mutant	5	traces[c]	nd
	10	25 ± 5[d]	∼60
	30	24 ± 5[d]	100
	50	30 ± 6[d]	100

[a]Conditions: 100 μM SOR, 3 mM 2-cyclohexen-1-ol, 0.4 M EtOH, 10 mM Tris/HCl, pH 8.5. Epoxide was detected by gas chromatography 2 min after the addition of H_2O_2. The reaction with H_2O_2 was carried out at room temperature and under anaerobic conditions (100% N_2 atmosphere). nd: not determined. [b]From UV−visible spectra analysis of the solution at 2 min reaction time. The spectra of the solution were recorded before and after K_2IrCl_6 treatments, to discriminate between reduced SOR, which exhibits an absorbance band in the 560−650 nm region after oxidation with K_2IrCl_6, and degraded SOR, which does not show any increase of absorbance in the 560−650 nm region after oxidation with K_2IrCl_6. Identical results were obtained in the presence or in the absence of 2-cyclohexen-1-ol. [c]Low amounts of epoxide were detected, which could not be accurately quantified. [d]Epoxide formed with a diastereoisomer excess of 20% for the *anti* isomers, corresponding to the enantiomers (1S,2R,6R) and (1R,2S,6S) 7-oxabicyclo[4-1-0] heptan 2-ol.

of SOR or in the presence of the wt protein or the E47A SOR mutant, no oxidation products of 2-cyclohexen-1-ol were detected (Table 2). On the other hand, in the presence of the K48I SOR mutant and 10−50 mol equiv of H_2O_2, 2-cyclohexen-1-ol was oxidized into epoxide, in a 25−30% yield, assuming a stoichiometric reaction of SOR with the olefin (Table 2). No other oxidation product, for example, the ketone 2-cyclohexen-1-one, was detected. The epoxide formed in the presence of the K48I SOR mutant contained a slight diastereoisomer excess of 20% for the *anti* isomers, corresponding to the enantiomers (1S,2R,6R) and (1R,2S,6S) 7-oxabicyclo[4-1-0] heptan 2-ol. When the reaction time was lengthened to 10 min, no variation in the amount of epoxide formed was observed (data not shown), showing that the oxidation reaction was over within 2 min.

UV−visible spectral analysis of the solution at 2 min reaction time revealed that the SOR active site got mostly destroyed, whether the olefin was present or not (wt and K48I SOR mutant proteins, Table 2). It should be noted that such denaturation processes precluded any possible turnover reactions in the oxidation of olefin.

These data demonstrate that the mutation of lysine 48 into isoleucine leads to new properties of SOR, allowing it to carry out $2e^-$ oxidation of organic substrates in the presence of H_2O_2. As was mentioned previously, the SOR active site is able to form iron peroxide species when treated with an excess of H_2O_2.[22−25] However, that an iron peroxide species in the K48I SOR mutant could be directly involved in the oxidation reaction is unlikely. In fact, such iron peroxide species were shown to be poor oxidant, not prone to carry out oxidation reaction of sulfide and olefin.[40,41,43] On the other hand, high-valent iron-oxo species, generated via O−O bond cleavage of the iron-peroxide species in iron complexes, are known to be the active species in the oxidation of organic substrates.[40−43] These data suggested that in the K48I SOR mutant, the Fe^{3+}−O−OH species formed upon reaction with H_2O_2 undergoes a cleavage of its O−O bond to generate an iron-oxo species. Whether this cleavage could be homolytic or heterolytic to generate $Fe(IV)=O$ + $HO^\bullet$ or $Fe(V)=O$ + HO^- species, respectively, is still unknown. Nevertheless, our data showed no evidence for the involvement of $HO^\bullet$ in the oxidation reaction. As a matter of fact, epoxidation reaction involves an oxygen transfer to a C−C double bond, corresponding to a $2e^-$ oxidation. One-electron oxidant species such as $HO^\bullet$ are not prone to carry out such reaction. In addition, the high chemoselectivity toward epoxidation and the presence of diastereoisomeric excess of the *anti* isomers are not in favor of a free radical chemistry. Thus, these data indicated for the K48I SOR mutant a metal-based mechanism, possibly an iron-oxo species directly involved in the $2e^-$ oxidation of 2-cyclohexen-1-ol. Hence, in the SOR from *D. baarsii*, the K48I mutation would favor formation of a highly oxidant iron-oxo species in its active site.

The demonstration that the K48I SOR mutant can perform oxidation reaction provides an explanation for the formation of a Fe^{2+} species without production of H_2O_2 at the end of the reaction of the mutant with $O_2^{\bullet-}$ (Figure 6 and Table 1). This Fe^{2+} species could result from a $2e^-$ oxidation reaction of organic solutes present in the solution used in pulse radiolysis, formate, tris-hydroxymethyl aminomethane, or glycine, carried out by a $Fe(IV)=O$ species formed through homolytic cleavage of an iron peroxide intermediate (Scheme 2).

These data highlight a pivotal role for K48 in the control of the evolution of the reaction intermediate during the reaction of SOR with $O_2^{\bullet-}$. This role is in full agreement with the X-ray structures of the iron peroxide species in SOR, which suggests the involvement of K48 in a specific protonation of the proximal oxygen of the iron hydroperoxide intermediate, to generate the reaction product H_2O_2.[25] Our data suggest that in the absence of K48, the protonation of the proximal oxygen of the peroxide intermediate does not occur, thus favoring a cleavage of the O−O bond of the iron peroxide intermediate to generate an iron-oxo species. In cytochrome P450, it has been shown that a hydrogen-bond network induced a double protonation of the distal oxygen of the iron peroxide intermediate, favoring the cleavage of the O−O bound of the peroxide moiety and formation of the high-valent iron-oxo species (compound **1**).[15] That such a double protonation of the

Scheme 2. Proposed Mechanism for the Reaction of SOR with $O_2^{\bullet -}$, Involving K48 in the Second Protonation Process[a]
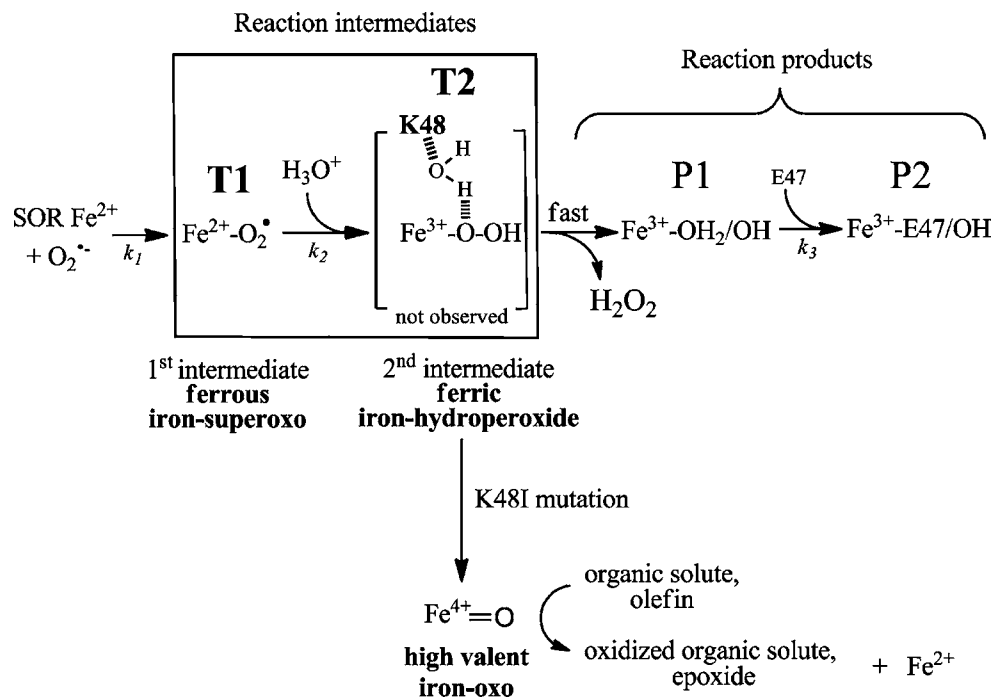
[a]T1 and T2, formulated as ferrous iron-superoxo and ferric iron hydroperoxide species, respectively, are the two reaction intermediates that lead to the formation of H_2O_2. T2 decays in a non-rate limiting step involving K48, and it is not observed by rapid kinetic studies.

distal oxygen of the peroxide might occur in the K48I SOR mutant is not known, but might be considered taking into account the solvent exposed active site of SOR and the presence of water molecule in the X-ray structure of SOR with the peroxide adduct hydrogen bonded to its distal oxygen atom.[25] Other factors, such as the spin state of the iron peroxide species, high spin for SOR[44,45] or low spin for cytochrome P450,[15] were also proposed to be important to control the evolution of the iron-peroxide intermediate. However, our results provide evidence for the ability of the SOR active site to form iron-oxo species and that the tight control of the protonation of the peroxide intermediate might be the determining factor to avoid formation of such highly oxidizing species.

The First Reaction Intermediate T1 Is a Ferrous Iron-superoxo Species: TD-DFT Calculation on Its Absorption Spectrum. Our present data showed that K48 is not involved in the unique protonation step observed by pulse radiolysis (Figure 2). These data suggest that K48 is involved in the second protonation step not observed in rapid kinetics. This step would be a fast, nonrate-limiting process, leading to the formation of a ferric iron hydroperoxide species, denoted T2 in Scheme 2. The structure of T2 could correspond to the X-ray structure of the iron peroxide intermediate trapped in monomer D in the crystal of SOR from *D. baarsii*, where a water molecule hydrogen bonded to K48 was closely positioned to the proximal oxygen of the hydroperoxide intermediate.[25] Such a conformation could be in agreement with a fast, nonrate-limiting protonation process by this water molecule of the hydroperoxide moiety to form H_2O_2. That such an instable species was trapped in the crystal could be associated with its stabilization by the local packing forces.[25]

The proposition of two protonation steps following the formation of T1 has also important consequences concerning the chemical structure of T1 (Scheme 2). T1, which resulted from the binding of $O_2^{\bullet -}$ to the sixth free coordination position of the ferrous iron center, has to be now formulated as a nonprotonated species. Consequently, T1 could be either a $Fe^{3+}-O-O^-$ or a $Fe^{2+}-O_2^{\bullet}$ species, depending on whether the electron transfer from the ferrous iron to the $O_2^{\bullet -}$ adduct occurred in this nonprotonated species. Interestingly, recent theoretical studies on SOR, using a Hubbard U correction to standard DFT calculations, suggested that $O_2^{\bullet -}$ could not be reduced to the peroxide species as a mere consequence of its binding to the active site of SOR.[46] According to ref 46, the reduction of $O_2^{\bullet -}$ would occur in a later step, assisted by proton transfer. We thus propose T1 as a ferrous iron-superoxo species (Scheme 2).

TD-DFT calculations were undertaken to investigate if a ferrous iron-superoxo species formed in the active site of SOR could exhibit an absorption band centered around 600 nm, as observed for the T1 intermediate (Figure 1). The model systems were taken from the crystallographic structure of the wt SOR from *D. baarsii* at 1.7 Å resolution.[25] To build the systems, only the five amino acids binding iron were taken into consideration, H49, H69, H75, H119, and C116. For the ferrous pentacoordinated state (Figure 7a), with iron at a formal oxidation degree of +II, quintet spin state ($S = 2$) was found to be the most stable, consistent with previous work.[46] In the optimized structure of the hexacoordinated state (Figure 7b), superoxide anion is bound to iron via one oxygen atom. In this second system, quartet and sextet ($S = 3/2$ and $S = 5/2$) structures were found to have very similar energies, as was previously reported in ref 46. We retained the sextet due to a smaller spin contamination. In the hexacoordinated state, superoxide moiety kept its radical characteristics with a total spin population of 1.05, consistent with an active site containing an $Fe^{2+}-OO^{\bullet}$ electronic arrangement. No $Fe^{3+}-$
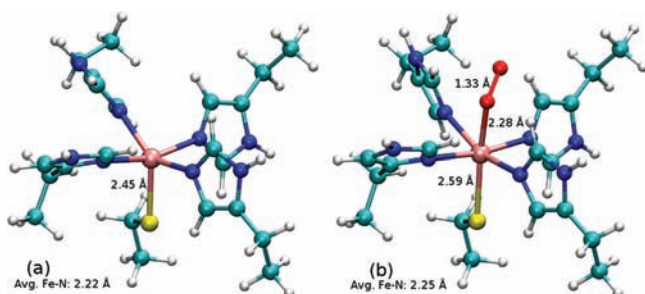
Figure 7. Optimized structures for reduced SOR (a) and reduced SOR with superoxide substrate (b); geometries optimized using the B3LYP/double-ζ level of theory.

OO^- arrangement could be characterized. Finally, 20 transitions were computed by means of the TD-DFT formalism (B3LYP/6-311+G**) for both of the structures presented in Figure 7.

The TD-DFT computed spectra are presented in Figure 8. Three transitions have appreciable oscillator strengths for the
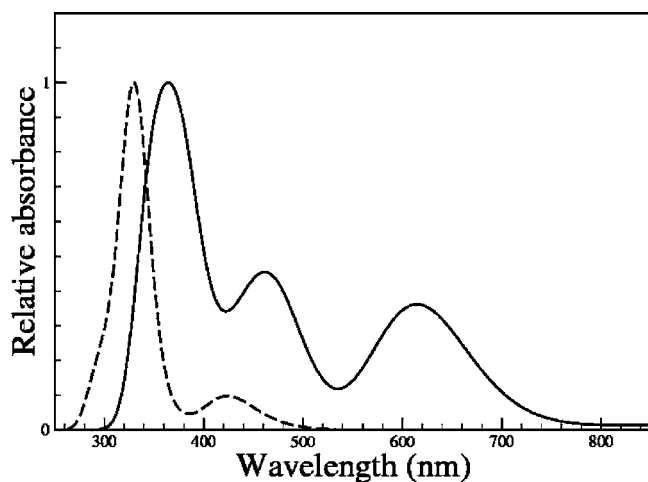

Figure 8. TD-DFT computed UV/vis spectra for the active site of SOR. (− − −) Pentacoordinated ferrous form (structure a, Figure 7). (−) Hexacoordinated ferrous form with a $O_2^{\bullet-}$ bound (structure b, Figure 7). Absorbance is given relative to the highest peak (value of 1).

ferrous pentacoordinated form and four in the case of the superoxide-bound SOR. The oscillator strengths, the orbitals involved, and the attribution of charge transfer were summarized in Supporting Information, Table S1. The two spectra showed a similar band around 350 nm (330 and 370 nm, respectively), attributed to a sulfur to iron charge transfer (Supporting Information Table S1). This is in agreement with ref 47, where in the case of reduced *Pyrococcus furiosus* SOR the bands at 31 200 and 33 900 cm^{-1} (295 and 320 nm, respectively) were assigned by MCD spectroscopy to a (Cys)S$^-$ → Fe^{2+} charge transfer. Addition of the superoxide to the pentacoordinated ferrous form led to two new bands at 614 and 475 nm (Figure 8), both attributed to charge transfer to the superoxide ligand. The 614 nm band could be assigned to a ferrous iron to superoxide charge transfer, while the 475 nm band would arise from a sulfur to superoxide charge transfer. This latter band occurred between the lone pair of the sulfur and the π^* orbital located on the superoxide ligand.

The experimental spectrum of T1 characterized in the 500−700 nm region (Figure 1), with a broad band centered around 600 nm, fits well with the ferrous iron to $O_2^{\bullet-}$ charge transfer band described by TD-DFT. These data support the proposition of T1 as a ferrous iron-superoxo species, as shown in Scheme 2.

Whereas iron ferric-superoxo species as reaction intermediates in some nonheme iron containing oxidase-oxygenases have been spectrocopically characterized,[48,49] to the best of our knowledge, no spectroscopic characterization for a ferrous iron-superoxo species has been reported to date. In the nonheme Fe^{2+} containing homoprotocatechuate 2,3 dioxygenase, one of the reaction intermediates has been proposed to be a Fe^{2+} superoxo species, based on X-ray diffraction studies.[50] This intermediate has been proposed to result from a one-electron transfer from the substrate chelated to the ferrous iron to O_2, hence forming substrate and oxygen radicals, which further recombine, conducting to oxygen insertion into the substrate.[51] In the case of SOR, the Fe^{2+} superoxo species, which results from the binding of $O_2^{\bullet-}$ on the ferrous ion, is not expected to prone such oxidation reactions.

■ CONCLUSIONS

In this work, we reinvestigated the reaction mechanism of the SOR from *D. baarsii* with $O_2^{\bullet-}$ and focused on the role of the K48 residue. We propose a new reaction scheme for the catalytic mechanism (Scheme 2), which redefines the chemical nature of the first reaction intermediate as an unprecedented ferrous iron superoxo species ($Fe^{2+}-O-O^{\bullet}$) and establishes an essential role for K48 in the control of the evolution of the iron peroxide intermediate to form the reaction product H_2O_2. The presence of K48 is shown to be an essential feature to avoid the formation of iron-oxo species, which would be otherwise formed in the SOR active site.

SOR catalysis has long been associated with the formation of a ferric iron peroxide intermediate, resulting from an inner sphere reduction mechanism of $O_2^{\bullet-}$ by the ferrous iron. The only catalytic competent reaction intermediate (T1) observed by pulse radiolysis was thus proposed to correspond to such an iron hydroperoxide species, which was further protonated to form H_2O_2. In fact, one protonation step was observed by pulse radiolysis following the formation of T1 and appeared to be consistent with such a reaction scheme.[18−20]

Our present results support a reformulation of the chemical nature of the T1 intermediate. We showed that, although the K48I mutation had no effect on T1 and on its protonation, it dramatically modified the reaction products, with no production of H_2O_2 and formation of a SOR ferrous form instead of a ferric one. In agreement with the recent X-ray structures of the peroxide intermediates trapped in a SOR crystal[25] and with the evidence that the K48I SOR mutant can form iron-oxo species (see below), our data strongly suggest that K48 is involved in a second protonation step, which is not observed in pulse radiolysis. This implies that T1 must be formulated as an unprotonated species, possibly a ferrous iron-superoxo species formed after the fast binding of $O_2^{\bullet-}$ on the ferrous iron. This is in agreement with recent theoretical calculations on SOR, which suggested that the electron transfer from the ferrous iron to $O_2^{\bullet-}$ to form the ferric iron peroxide intermediate is dependent on a further protonation on the $O_2^{\bullet-}$ moiety.[46] Our TD-DFT calculations fully supported this hypothesis in that the calculations showed that such a ferrous iron superoxo intermediate would present a broad absorption band at 614 nm, which is very similar to the spectrum of T1 observed by pulse radiolysis. This absorption band was assigned

to a ferrous iron to $O_2^{\bullet-}$ charge transfer, and, to our knowledge, an absorption band for such an iron species has never been described in the literature. Characterization of a ferrous iron-superoxo intermediate species is unprecedented in metalloenzymes.

According to our new reaction scheme (Scheme 2), the ferrous iron-superoxo intermediate is protonated by H^+ from the bulk to form a second reaction intermediate, the ferric iron hydroperoxide species. This second reaction intermediate does not accumulate because, as suggested by the X-ray structure of monomer D,[25] the hydrogen-bond network involving K48 positions a water molecule in close proximity to the proximal oxygen of the iron hydroperoxide, allowing a very fast and pH-independent protonation process to generate H_2O_2. Thus, the new proposed reaction mechanism of SOR with $O_2^{\bullet-}$ involves two reaction intermediates, a ferrous iron superoxo and a ferric iron hydroperoxide species (Scheme 2).

In this reaction mechanism, the specificity of the protonation of the iron hydroperoxide intermediate appears to be a key step for the SOR activity. This is illustrated by the fact that the K48I SOR mutant exhibits a new catalytic property and is able to carry out a $2e^-$ oxidation of olefin in the presence of H_2O_2 to form epoxide. These data strongly support the fact that the active site of the K48I SOR mutant forms a high valent iron-oxo species, which is directly responsible for the $2e^-$ oxidation of olefin. Such formation of a high valent iron-oxo species is also fully consistent with the effect of the K48I mutant on the reaction of SOR with $O_2^{\bullet-}$, as observed by pulse radiolysis. These data suggest that in the absence of the K48 residue, the iron peroxide intermediate evolves toward a cleavage of its O—O bond to form an iron-oxo species. This is in agreement with the absence of a specific protonation of the proximal oxygen in the K48I SOR mutant, as illustrated by the X-ray structure of the iron peroxide intermediates.[25]

Then, these data highlight a pivotal role of K48 in SOR catalysis, which allows for a tight control of the evolution of the iron peroxide intermediate toward the formation of H_2O_2.

Although it was proposed that a high-spin state was a determining factor to favor the cleavage of the iron-peroxide Fe—O bond to generate H_2O_2,[44,45] our results show that the O—O bond cleavage is possible despite the existence of a high-spin iron peroxide intermediate at the nonheme $[FeN_4S_1]$ center of SOR.

This work illustrates an example of how an enzyme, SOR, can use reaction intermediate typical of oxygenase enzymes, for example, iron hydroperoxide species, to carry out antioxidant activity and $O_2^{\bullet-}$ detoxification.

■ ASSOCIATED CONTENT

ⓢ Supporting Information

Relevant transitions by the mean of TD-DFT for the ferrous SOR, penta-coordinated, and hexa-coordinated (SOR–$O_2^{\bullet-}$) structures (Table S1). Complete ref 30. This material is available free of charge via the Internet at http://pubs.acs.org.

■ AUTHOR INFORMATION

Corresponding Author
vniviere@cea.fr

Notes
The authors declare no competing financial interest.

■ REFERENCES

(1) Imlay, J. A. *Annu. Rev. Biochem.* **2008**, *77*, 755−776.
(2) Winterbourn, C. C. *Nat. Chem. Biol.* **2008**, *4*, 278−286.
(3) Fridovich, I. *Annu. Rev. Biochem.* **1995**, *64*, 97−112.
(4) Jenney, F. E. Jr.; Verhagen, M. F. J. M.; Cui, X.; Adams, M. W. W. *Science* **1999**, *286*, 306−309.
(5) Lombard, M.; Fontecave, M.; Touati, D.; Nivière, V. *J. Biol. Chem.* **2000**, *275*, 115−121.
(6) Emerson, J. P.; Coulter, E. D.; Phillips, R. S.; Kurtz, D. M. Jr. *J. Biol. Chem.* **2003**, *278*, 39662−39668.
(7) Santos-Silva, T.; Trincao, J.; Carvalho, A. L.; Bonifacio, C.; Auchère, F.; Raleiras, P.; Moura, I.; Moura, J. J. G.; Romao, J. *J. Biol. Inorg. Chem* **2006**, *11*, 548−558.
(8) Grunden, A. M.; Jenney, F. E. Jr.; Ma, K.; Ji, M.; Weinberg, M. V.; Adams, M. W. W. *Appl. Environ. Microbiol.* **2005**, *71*, 1522−1530.
(9) Kurtz, D. M. Jr. *Acc. Chem. Res.* **2004**, *37*, 902−908.
(10) Pereira, A. S.; Tavares, P.; Folgosa, F.; Almeida, R. M.; Moura, I.; Moura, J. J. G. *Eur. J. Inorg. Chem.* **2007**, *18*, 2569−2581.
(11) Pinto, A. F.; Rodrigues, J. V.; Teixeira, M. *Biochim. Biophys. Acta* **2010**, *1804*, 285−297.
(12) Nivière, V.; Bonnot, F.; Bourgeois, D. In *Handbook of Metalloproteins,* ; Messerschmidt, A., Ed.; John Wiley & Sons, Ltd.: Chichester, UK, 2011; Vols. 4 & 5, Superoxide reductase, pp 246−258.
(13) Yeh, A. P.; Hu, Y.; Jenney, F. E. Jr.; Adams, M. W. W.; Rees, D. C. *Biochemistry* **2000**, *39*, 2499−2508.
(14) Coelho, A.; Matias, P.; Fülöp, V.; Thompson, A.; Gonzalez, A.; Carrondo, M. A. *J. Biol. Inorg. Chem.* **1997**, *2*, 680−689.
(15) Denisov, I. G.; Makris, T. M.; Sligar, S. G.; Schlichting, I. *Chem. Rev.* **2005**, *105*, 2253−2277.
(16) Folgosa, F.; Cordas, C. M.; Santos, J. A.; Pereira, A. S.; Moura, J. J.; Tavares, P. A.; Moura, I. *Biochem. J.* **2011**, *438*, 485−494.
(17) Bonnot, F.; Duval, S.; Lombard, M.; Valton, J.; Houée-Levin, C.; Nivière, V. *J. Biol. Inorg. Chem.* **2011**, *16*, 889−896.
(18) Emerson, J. P.; Coulter, E. D.; Cabelli, D. E.; Phillips, R. S.; Kurtz, D. M. Jr. *Biochemistry* **2002**, *41*, 4348−4357.
(19) Nivière, V.; Asso, M.; Weill, C. O.; Lombard, M.; Guigliarelli, B.; Favaudon, V.; Houée-Levin, C. *Biochemistry* **2004**, *43*, 808−818.
(20) Rodrigues, J. V.; Abreu, I. A.; Cabelli, D. E.; Teixeira, M. *Biochemistry* **2006**, *45*, 9266−9278.
(21) Bonnot, F.; Houée-Levin, C.; Favaudon, V.; Nivière, V. *Biochim. Biophys. Acta* **2010**, *1804*, 762−767.
(22) Mathé, C.; Mattioli, T. A.; Horner, O.; Lombard, M.; Latour, J. M.; Fontecave, M.; Nivière, V. *J. Am. Chem. Soc.* **2002**, *124*, 4966−4967.
(23) Mathé, C.; Nivière, V.; Mattioli, T. A. *Biophys. Chem.* **2006**, *119*, 38−48.
(24) Mathé, C.; Weill, C. O.; Mattioli, T. A.; Berthomieu, C.; Houée-Levin, C.; Tremey, E.; Nivière, V. *J. Biol. Chem.* **2007**, *282*, 22207−22216.
(25) Katona, G.; Carpentier, P.; Nivière, V.; Amara, P.; Adam, V.; Ohana, J.; Tsanov, N.; Bourgeois, D. *Science* **2007**, *316*, 449−453.
(26) Kitagawa, T.; Dey, A.; Lugo-Mas, P.; Benedict, J. B.; Kaminsky, W.; Solomon, E.; Kovacs, J. A. *J. Am. Chem. Soc.* **2006**, *128*, 14448−14449.
(27) Von Sonntag, C. *The Classical Basis of Radiation Biology*; Taylor and Francis: London, 1987.
(28) Mottola, H. A.; Simpson, B. E.; Gorin, G. *Anal. Chem.* **1970**, *40*, 410−411.
(29) Freccero, M.; Gandolfi, R.; Sarzi-Amade, M.; Rastelli, A. *J. Org. Chem.* **2000**, *65*, 8948−8959.
(30) Frisch, M. J.; et al. *Gaussian 03*, revision B.05; Gaussian, Inc.: Wallingford, CT, 2004.

(31) Becke, A. D. *Chem. Phys.* **1993**, *98*, 5648−5652.

(32) Lee, C.; Yang, W.; Parr, R. G. *Phys. Rev. B* **1988**, *37*, 785−789.

(33) Hay, P. J.; Wadt, W. R. *J. Chem. Phys.* **1985**, *82*, 270−283.

(34) Bauernschmitt, R.; Ahlrichs, R. *Chem. Phys. Lett.* **1996**, *256*, 454−464.

(35) Casida, M. E.; Jamorski, C.; Casida, K. C.; Salhu, D. R. *J. Chem. Phys.* **1998**, *108*, 4439−4449.

(36) Cancès, M. T.; Mennucci, B.; Tomasi, J. *J. Chem. Phys.* **1997**, *107*, 3210−3221.

(37) As reported for the SOR from *D. vulgaris* Hildenborough (Huang, V. W.; Emerson, J. P.; Kurtz, D. M. Jr. *Biochemistry* **2007**, *46*, 11342−11351), the presence of a high concentration of formate/formic acid in the pulse radiolysis experiments induced a general acid catalysis on the decay of T1 for the wt, E47A, and K48I SORs from *D. baarsii* (data not shown). However, in the presence of 10 mM of formate and within the pH range studied here, this effect was found to be negligible on the k_2 values determined for the wt, E47A, and K48I SORs..

(38) Mathé, C.; Nivière, V.; Mattioli, T. A. *J. Am. Chem. Soc.* **2005**, *127*, 16436−14441.

(39) Dey, A.; Jenney, F. E. Jr.; Adams, M. W.; Johnson, M. K.; Hodgson, K. O.; Hedman, B.; Solomon, E. I. *J. Am. Chem. Soc.* **2007**, *129*, 12418−12431.

(40) Nam, W. *Acc. Chem. Res.* **2007**, *40*, 522−531.

(41) Que, L. Jr.; Tolman, W. B. *Nature* **2008**, *455*, 333−340.

(42) Kovaleva, E. G.; Lipscomb, J. D. *Nat. Chem. Biol.* **2008**, *4*, 186−193.

(43) Park, M.; Lee, J.; Suh, Y.; Kim, J.; Nam, W. *J. Am. Chem. Soc.* **2006**, *128*, 2630−2634.

(44) Brines, L. M.; Kovacs, J. A. *Eur. J. Inorg. Chem.* **2007**, *1*, 29−38.

(45) Bukowski, M. R.; Halfen, H. L.; van den Berg, T. A.; Halfen, J. A.; Que, L. Jr. *Angew. Chem., Int. Ed.* **2005**, *44*, 584−587.

(46) Sit, P. H.-L.; Migliore, A.; Ho, M. H.; Klein, M. L. *J. Chem. Theory Comput.* **2010**, *6*, 2896−2909.

(47) Clay, M. D.; Jenney, F. E. Jr.; Hagedoorn, P. L.; George, G. N.; Adams, M. W. W.; Johnson, M. K. *J. Am. Chem. Soc.* **2002**, *124*, 788−805.

(48) Mbughuni, M. M.; Chakrabarti, M.; Hayden, J. A.; Bominaar, E. L.; Hendrich, M. P.; Münck, E.; Lipscomb, J. D. *Proc. Natl. Acad. Sci. U.S.A.* **2010**, *107*, 16788−16793.

(49) Mukherjee, A.; Cranswick, M. A.; Chakrabarti, M.; Paine, T. K.; Fujisawa, K.; Münck, E.; Que, L. Jr. *Inorg. Chem.* **2010**, *49*, 3618−3628.

(50) Kovaleva, E. G.; Lipscomb, J. D. *Science* **2007**, *316*, 453−457.

(51) Kovaleva, E. G.; Neibergall, M. B.; Chakrabarty, S.; Lipscomb, J. D. *Acc. Chem. Res.* **2007**, *40*, 475−483.